Rolling along a square path: The dynamics of biased balls

Michael S. Wheatland, Rodney C. Cross, Andrew Ly, Michael Sacks, and Karl Smith

Rolling along a square path: The dynamics of biased balls

Michael S. Wheatland,[a] Rodney C. Cross,[b] Andrew Ly, Michael Sacks, and Karl Smith
School of Physics, The University of Sydney, New South Wales 2006, Australia

A biased ball rolled and spun on a horizontal surface exhibits interesting dynamics. We investigate the motion of a truncated billiard ball, via experiments, analytical methods, and numerical solutions of the equations of motion for a biased sphere rolling without slipping. Solutions are identified where the center of mass moves in a circular or a square path, and we investigate other quasi-periodic motions of the ball. © *2020 American Association of Physics Teachers.*
https://doi.org/10.1119/10.0000905

I. INTRODUCTION

Biased balls rolled and spun on a horizontal surface exhibit interesting and sometimes curious, unexpected dynamics. For example, a biased ball can roll along a circular path, but it can also roll along a square or triangular path. The torque produced by an offset center of mass causes a biased ball to depart from a straight line when rolling. A familiar example is provided by a lawn bowl, which generally rolls in a leisurely arc, but may also wobble as it rolls.[1–3] In general, the motion involves rotations about three axes: a spin about the symmetry axis of the bowl; a slow precession (the rotation of the symmetry axis about the vertical as the ball curves); and a nutation (the wobble of the axis up and down). The bowl rolls without slipping, and so the point of contact with the ground is instantaneously at rest.

A second example of the motion of a biased rolling ball is provided by hurricane balls, which consist of two bearing balls joined together.[4] When the balls are spun rapidly on a surface, they quickly achieve a steady state in which one ball is rolling without slipping, the center of mass is at rest, and the second ball is lifted off the surface. In this case, the center of mass of the system is the point at which the balls are joined, and so it is at the edge of the lower, rolling ball. The center of mass of the lower ball, which can be considered a biased rolling ball, moves in a circle.

The dynamics of biased balls have previously also been analysed theoretically and experimentally. Studies have looked at tippe tops, spheroids,[5] and a small ball connected to a larger ball.[6] In this paper, we will focus on a truncated sphere: a sphere with a part removed by a taking a planar slice through the sphere. The motion of a rolling truncated sphere has previously been investigated theoretically, under the restrictive assumption of zero spin about a vertical axis[7] (a "rubber body" model). In this paper, we provide a more general description of the motion of a rolling truncated sphere.

The present investigation was motivated in part by some interesting observations concerning the dynamics of a metal ring spun about a vertical axis. Several authors have reported a surprising effect, where the center of mass rotates initially in a prograde sense about a remote vertical axis and then changes direction to rotate in a retrograde sense before it comes to a stop.[8,9] The authors provided numerical solutions but were not able to explain the effect in simple terms.

In the present paper, we investigate experimentally the motion of a biased ball under conditions where the ball rotates about its axis of symmetry and also rotates about a vertical axis through its center of mass, G. Rotation about the symmetry axis is generated as a result of rolling motion, while an arbitrary rotation frequency about a vertical axis can be imposed by spinning the ball in that manner, a technique commonly employed in ten-pin bowling.[10,11] In ten-pin bowling, the center of mass generally rotates at low frequency about a remote vertical axis in a prograde sense, with a large radius of curvature. That is, the direction of rotation about the remote axis is in the same direction as rotation about the vertical axis through G. In our case, a billiard ball was biased by removing a portion of the ball, with the result that the ball curved in a retrograde sense. That is, the direction of rotation about the remote axis was in the opposite direction to that about the vertical axis through G. The radius of curvature was relatively small since the ball was launched at low speed.

A wide range of trajectories can be generated by varying the spin about the vertical axis and also by varying the inclination of the axis of symmetry. A representative sample of trajectories is presented below, including the case that the ball rolls along an almost square path. The trajectories were calculated numerically and are compared with the experimental results obtained with the truncated billiard ball. One particular mode is omitted from discussion in this paper since it has been described elsewhere and also because it requires slipping.[12] That is, if a truncated ball is spun at sufficiently high speed, it can completely invert like a tippe top.

II. MODEL

Here, we present a model for a rolling axisymmetric biased ball, following an approach used to describe a lawn bowl.[1,2] Figure 1 illustrates the ball geometry. A set of moving axes $G\xi\eta\zeta$ is chosen so that G is the center of mass of the ball, η is aligned with the axis of symmetry of the ball, and the axis ξ is always horizontal. In Fig. 1, the ξ-axis is directed into the page. The axes $G\xi\eta\zeta$ are aligned with and move with the ball, but are not fixed in the ball: The ball rotates about the η-axis as it rolls. The ball has radius a, and the center of mass is offset by a distance c from the center. The position and orientation of the ball in a frame $Oxyz$ fixed in the rolling surface is then defined by the position (x, y, z) of G, and the Euler angles θ, χ, and ϕ, where θ is the angle between ζ and z, χ is the angle between the x and ξ directions, and ϕ is an azimuthal angle around η, measured from ξ.

From Fig. 1, we can see that the angular velocity $\boldsymbol{\omega}$ of the ball is given by

$$\boldsymbol{\omega} = -\dot{\theta}\,\hat{\boldsymbol{\xi}} + \left(\dot{\phi} - \dot{\chi}\sin\theta\right)\hat{\boldsymbol{\eta}} + \dot{\chi}\cos\theta\,\hat{\boldsymbol{\zeta}}. \tag{1}$$
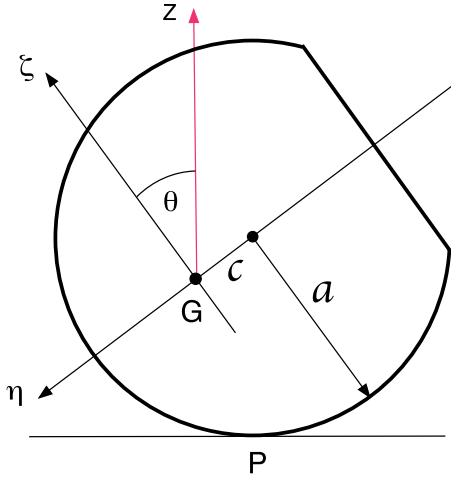
Fig. 1. Geometry of the model for a rolling biased ball. We consider axes ξ, η, and ζ through the center of mass G of the ball, which move with the ball. The axis η is aligned with the symmetry axis of the ball, and the axis ξ, which is directed into the page in the figure, remains horizontal.

The axes $G\xi\eta\zeta$ coincide with the principal axes of the ball, so the angular momentum of the ball is

$$
\begin{aligned}
\boldsymbol{L} &= A\omega_\xi \hat{\boldsymbol{\xi}} + B\omega_\eta \hat{\boldsymbol{\eta}} + A\omega_\zeta \hat{\boldsymbol{\zeta}}, \\
&= -A\dot\theta\,\hat{\boldsymbol{\xi}} + B(\dot\phi - \dot\chi \sin\theta)\,\hat{\boldsymbol{\eta}} + A\dot\chi \cos\theta\,\hat{\boldsymbol{\zeta}}, \quad (2)
\end{aligned}
$$

where B is the moment of inertia for rotation about the symmetry axis, and A is the second principal moment of inertia.

We can transform a vector with components in ξ, η, and ζ to a vector with components in x, y, and z by multiplying by the matrix

$$
\Lambda = \begin{pmatrix}
\cos\chi & -\cos\theta \sin\chi & -\sin\theta \sin\chi \\
\sin\chi & \cos\theta \cos\chi & \sin\theta \cos\chi \\
0 & -\sin\theta & \cos\theta
\end{pmatrix}, \quad (3)
$$

so that, e.g., the vector $\Lambda\boldsymbol{\omega}$ has components $(\omega_x, \omega_y, \omega_z)$, where $\boldsymbol{\omega} = (\omega_\xi, \omega_\eta, \omega_\zeta)$.

We assume that the ball rolls without slipping, which implies

$$
\boldsymbol{v} + \Lambda\boldsymbol{\omega} \times \mathbf{r}_{GP} = 0, \quad (4)
$$

where $\boldsymbol{v} = (\dot x, \dot y, \dot z)$ is the center of mass velocity and

$$
\begin{aligned}
\mathbf{r}_{GP} &= -c\hat{\boldsymbol{\eta}} - a\hat{z}, \\
&= (c\cos\theta \sin\chi, -c\cos\theta \cos\chi, -a + c\sin\theta) \quad (5)
\end{aligned}
$$

is the vector from the center of mass G to the point P in contact with the surface.

Equation (4) is a kinematic relationship, which defines the motion of the ball's center of mass in terms of the Euler angles. From Eqs. (1) and (3)–(5), it follows that

$$
\dot x = (a\dot\phi - c\dot\chi)\cos\theta \cos\chi - (a - c\sin\theta)\dot\theta \sin\chi, \quad (6)
$$

$$
\dot y = (a\dot\phi - c\dot\chi)\cos\theta \sin\chi + (a - c\sin\theta)\dot\theta \cos\chi, \quad (7)
$$

$$
\dot z = -c\cos\theta\,\dot\theta. \quad (8)
$$

The last equation can be directly integrated to give

$$
z = a - c\sin\theta, \quad (9)
$$

using the condition $z = a$ when $\theta = 0$.

Again using the fact that the axes $G\xi\eta\zeta$ coincide with the principal axes of the ball, the kinetic energy T is given by

$$
T = \frac{1}{2}A\omega_\xi^2 + \frac{1}{2}B\omega_\eta^2 + \frac{1}{2}A\omega_\zeta^2 + \frac{1}{2}M(\dot x^2 + \dot y^2 + \dot z^2), \quad (10)
$$

where M is the ball's mass. Using Eqs. (1) and (6)–(8) leads to

$$
\begin{aligned}
T = &\frac{1}{2}A\left(\dot\theta^2 + \dot\chi^2 \cos^2\theta\right) + \frac{1}{2}B\left(\dot\phi - \dot\chi \sin\theta\right)^2 \\
&+ \frac{1}{2}M\left[(a\dot\phi - c\dot\chi)^2 \cos^2\theta + (a^2 - 2ac\sin\theta + c^2)\dot\theta^2\right].
\end{aligned} \quad (11)
$$

Also, the potential energy of the ball is

$$
V = mg(a - c\sin\theta). \quad (12)
$$

The equations of motion may be obtained using the Lagrangian method with the non-holonomic constraints implied by the rolling conditions Eqs. (6)–(8). The details are given in Appendix A. The results are

$$
\begin{aligned}
&[A + M(a^2 - 2ac\sin\theta + c^2)]\ddot\theta - Mac\cos\theta\,\dot\theta^2 \\
&\quad - [(B - A)\sin\theta + Mc(a - c\sin\theta)]\cos\theta\,\dot\chi^2 \\
&\quad + [B + Ma(a - c\sin\theta)]\cos\theta\,\dot\phi\,\dot\chi - Mgc\cos\theta = 0,
\end{aligned} \quad (13)
$$

$$
\begin{aligned}
&[(A + Mc^2)\cos^2\theta + B\sin^2\theta]\ddot\chi - (B\sin\theta + Mac\cos^2\theta)\ddot\phi \\
&\quad + [2(B - A - Mc^2)\sin\theta + Mac]\cos\theta\,\dot\theta\,\dot\chi \\
&\quad - (B - Mac\sin\theta)\cos\theta\,\dot\theta\,\dot\phi = 0,
\end{aligned} \quad (14)
$$

$$
\begin{aligned}
&-(B\sin\theta + Mac\cos^2\theta)\ddot\chi + (B + Ma^2\cos^2\theta)\ddot\phi \\
&\quad - (B - 2Mac\sin\theta + Ma^2)\cos\theta\,\dot\theta\,\dot\chi \\
&\quad - Ma^2\sin\theta\cos\theta\,\dot\theta\,\dot\phi = 0.
\end{aligned} \quad (15)
$$

Equations (13)–(15) together with Eqs. (6)–(8) describe the motion of the ball.

The force acting on the ball (for general motion) is $\boldsymbol{F} = M(\ddot x, \ddot y, \ddot z)$, which may be calculated from Eqs. (6)–(8),

$$
\begin{aligned}
\ddot x = &(a\ddot\phi - c\ddot\chi)\cos\theta \cos\chi - (a\dot\phi - c\dot\chi) \\
&\times (\sin\theta \cos\chi\,\dot\theta + \cos\theta \sin\chi\,\dot\chi) \quad (16)
\end{aligned}
$$

$$
+ c\cos\theta \sin\chi(\dot\theta)^2 - (a - c\sin\theta)(\sin\chi\,\ddot\theta + \cos\chi\,\dot\theta\dot\chi), \quad (17)
$$

$$
\begin{aligned}
\ddot y = &(a\ddot\phi - c\ddot\chi)\cos\theta \sin\chi + (a\dot\phi - c\dot\chi) \\
&\times (-\sin\theta \sin\chi\,\dot\theta + \cos\theta \cos\chi\,\dot\chi) \quad (18)
\end{aligned}
$$

$$
- c\cos\theta \cos\chi(\dot\theta)^2 + (a - c\sin\theta)(\cos\chi\,\ddot\theta - \sin\chi\,\dot\theta\dot\chi), \quad (19)
$$

$$
\ddot z = c[\sin\theta(\dot\theta)^2 - \cos\theta\,\ddot\theta]. \quad (20)
$$

Similarly, the net torque on the ball may be calculated as

$$\boldsymbol{\tau} = \mathbf{r}_{GP} \times \left(F_x \hat{\mathbf{x}} + F_y \hat{\mathbf{y}} + N \hat{\mathbf{z}} \right), \tag{21}$$

where $N - Mg = F_z$. This gives

$$\tau_x = -m(g + \ddot{z})c\cos\theta\cos\chi - m\ddot{y}(-a + c\sin\theta), \tag{22}$$

$$\tau_y = m\ddot{x}(-a + c\sin\theta) - m(g + \ddot{z})c\cos\theta\sin\chi, \tag{23}$$

$$\tau_z = mc\cos\theta(\ddot{y}\sin\chi + \ddot{x}\cos\chi). \tag{24}$$

III. STEADY-STATE SOLUTIONS

Steady-state solutions correspond to

$$\ddot{\theta} = \ddot{\chi} = \ddot{\phi} = 0. \tag{25}$$

If the ball rolls with a constant inclination of the axis to the vertical ($\dot{\theta} = 0$), then we have

$$\theta = \theta_c, \quad \chi = \Omega_c t, \quad \phi = \omega_c t, \tag{26}$$

where θ_c, Ω_c, and ω_c are constant and where we have chosen $\chi = \phi = 0$ at time $t = 0$. The angular velocity Ω_c represents the rate at which the moving frame $G\xi\eta\zeta$ aligned with the ball rotates about a vertical axis through the ball's center of mass, and ω_c is the rate at which the ball rotates about the η-axis as it rolls (see Fig. 1). With these choices, Eqs. (14) and (15) become trivial, and Eq. (13) reduces to

$$-\left[(B - A)\sin\theta_c + Mc(a - c\sin\theta_c) \right] \Omega_c^2 \\ + \left[B + Ma(a - c\sin\theta_c) \right] \omega_c \Omega_c - Mgc = 0, \tag{27}$$

assuming $\cos\theta_c \neq 0$. We can also rewrite this equation as

$$\omega_c = \frac{Mgc + \left[(B - A)\sin\theta_c + Mc(a - c\sin\theta_c) \right] \Omega_c^2}{[B + Ma(a - c\sin\theta_c)]\Omega_c}. \tag{28}$$

The rolling conditions [Eqs. (6)–(8)] imply

$$\dot{x} = v_c \cos(\Omega_c t), \tag{29}$$

$$\dot{y} = v_c \sin(\Omega_c t), \tag{30}$$

$$\dot{z} = 0, \tag{31}$$

where

$$v_c = (a\omega_c - c\Omega_c)\cos\theta_c. \tag{32}$$

Equations (29)–(31) may be integrated to give

$$x - x_0 = R\sin(\Omega_c t), \tag{33}$$

$$y - y_0 = -R\cos(\Omega_c t), \tag{34}$$

$$z = a - c\sin\theta, \tag{35}$$

where x_0 and y_0 are the integration constants and

$$R = v_c / \Omega_c. \tag{36}$$

Equations (33)–(34) describe uniform circular motion in x and y centered on (x_0, y_0) with radius R. The ball rolls in a circle with a constant inclination of the spin axis to

the vertical, with the sense of rotation determined by the sign of Ω_c.

The spin frequency ω_c may be eliminated between Eqs. (27) and (36) to give

$$\Omega_c^2 = \frac{Mgac\cos\theta_c}{B(R + c\cos\theta_c) + MaR(a - c\sin\theta_c) - a(B - A)\sin\theta_c\cos\theta_c}, \tag{37}$$

and then Eq. (36) implies

$$\omega_c = \frac{\Omega_c}{a}\left(\frac{R}{\cos\theta_c} + c \right). \tag{38}$$

From Eqs. (22)–(24), the torque is given by $\tau_z = 0$ and

$$\tau_x = \tau_c \cos(\Omega_c t), \quad \tau_y = \tau_c \sin(\Omega_c t), \tag{39}$$

where

$$\tau_c = m\cos\theta_c\left[-gc + (a - c\sin\theta_c)(a\omega_c - c\Omega_c)\Omega_c \right]. \tag{40}$$

The torque is constant in magnitude, horizontal, and parallel or anti-parallel to the velocity of the ball. The torque induces precessional motion, with the result that the center of mass follows a circular path, the torque being equal to the rate of change of angular momentum.

If the center of mass is at rest then $R = 0$. In that case, Eq. (36) implies

$$a\omega_c = c\Omega_c, \tag{41}$$

which is the no-slip condition for a stationary center of mass.

In the game of lawn bowls, θ_c is usually zero, in which case Eqs. (37) and (38) simplify to give $(R + c)\Omega_c = a\omega_c$ and

$$\Omega_c^2 = \frac{Mgac}{B(R + c) + Ma^2 R}. \tag{42}$$

IV. NUMERICAL METHOD

For numerical solution, the equations of motion are written in the form $d\boldsymbol{u}/dt = \boldsymbol{f}$, where

$$\boldsymbol{u} = \left(x, y, \theta, \chi, \phi, \dot{\theta}, \dot{\chi}, \dot{\phi} \right) \tag{43}$$

and

$$\boldsymbol{f} = \left(\dot{x}, \dot{y}, \dot{\theta}, \dot{\chi}, \dot{\phi}, \ddot{\theta}, \ddot{\chi}, \ddot{\phi} \right). \tag{44}$$

The equations are also non-dimensionalised by dividing lengths by a, times by $\sqrt{a/g}$, and moments of inertia by Ma^2. In this form, the equations are solved for the dependent variables $\boldsymbol{u}$ at a set of time steps using fourth order Runge–Kutta.[13] The acceleration terms (the second derivatives of the Euler angles) in $\boldsymbol{f}$ are evaluated at each timestep using Eqs. (13)–(15), including solving a linear system of equations at each time step. Further details are given in Appendix B.

The code implementing the numerical solution requires initial conditions $\theta(t = 0) = \theta_0$, $\dot{\theta}(t = 0) = \dot{\theta}_0$, $\chi(t = 0) = \chi_0$, and $\dot{\phi}(t = 0) = \dot{\phi}_0$. The initial values of the angles χ

and ϕ can be assumed to be zero although a non-zero χ can be used to rotate the trajectory of the ball in the xy-plane. The time step is chosen so that it is initially less than $2\pi/\dot{\theta}_0$, $2\pi/\dot{\chi}_0$, and $2\pi/\dot{\phi}_0$, in the case that the initial angular velocities are non-zero. The code integrates for a chosen total time, and it produces a visualisation of the motion of the ball.

As a check on the numerical calculation, we evaluate the total energy $E = T + V$ using Eqs. (11) and (12) and ensure that it is close to being conserved during the integration time. The forces and torques acting on the ball are also calculated, using Eqs. (16)–(19) and (22)–(24), respectively.

V. EXPERIMENTAL METHOD

The top 12 mm of a two inch (50.8 mm) diameter billiard ball was removed to shift the center of mass by 2.9 mm from the geometric center of the ball, as shown in Fig. 2. The mass of the ball was thereby reduced to 98.4 g, giving $A = 2.39 \times 10^{-5}$ kg m^2 and $B = 2.69 \times 10^{-5}$ kg m^2. A thin wire probe was inserted in the center of the flat section so that the center of mass could be located by extrapolating the measured coordinates of the top and bottom of the probe. When viewed from above, the apparent length of the probe was used to calculate the angle of inclination of the probe from the vertical, and the angular displacement of the probe in the horizontal plane was used to calculate the precession frequency $\Omega = \dot{\chi}$ of the ball.

The ball was launched by hand at low speed on an accurately horizontal and flat granite surface measuring 30 cm × 30 cm, and was filmed from above at 300 fps with a Casio EX-F1 camera mounted on a tripod. The video was analysed with Tracker motion analysis software to measure the trajectory and speed of the center of mass in the horizontal plane, as well as the inclination angle, θ, and the precession frequency, Ω. We did not attempt to measure the spin frequency $\omega = \dot{\phi}$. Typical results are shown in four supplementary videos.[14]

VI. EXPERIMENTAL AND NUMERICAL RESULTS

A. Lawn bowl mode

A relatively simple result was obtained by launching the ball at low speed with the axis of symmetry approximately horizontal and without imparting any deliberate rotation
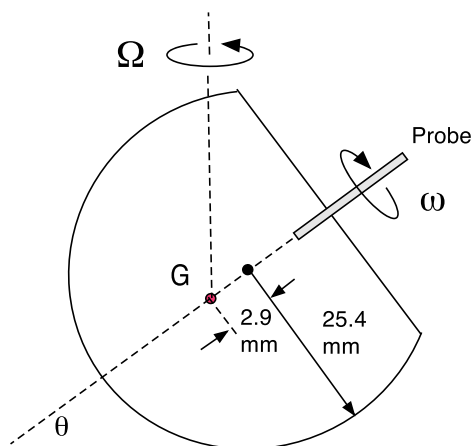
about a vertical axis. That is, the usual method of launching a ball in lawn bowls. The result, shown in Fig. 3, corresponds to the steady-state circular motion solution described in Sec. III. The center of mass follows a circular path of radius $R = 0.073$ m, completing one orbit in time $T = 1.95$ s at an average speed $v = 0.235$ m/s and at angular velocity $|\Omega| = 2\pi/T = 3.22$ rad/s. The average angle of inclination, θ, was 24°, giving a theoretical precession frequency (from Eq. (37)) of $|\Omega| = 3.23$ rad/s.

The circular motion solution provides a simple test for our code. In Fig. 4, we show the numerical integration of the equations of motion for initial values $\theta_0 = 24°$, $\dot{\theta}_0 = 0$, $\dot{\chi}_0 = -3.23$ rad/s, and with $\dot{\phi}_0 \approx -10.16$ rad/s, evaluated using Eq. (28). The initial position is taken to be $x = 0$, $y = -R$, with R given in Eqs. (32) and (36) using $\Omega_c = \dot{\chi}_0$. As expected, these initial conditions produce a steady state with the ball rolling clockwise in a circle centered on the origin, and moreover, reproduce the experimental results shown in Fig. 3. Figure 4(a) shows the result of the numerical calculation. A visualisation of the solution, which animates the rolling ball during the motion, is provided as supplementary material.[14] The red curve in Fig. 4(a) is the path of the center of mass, the blue curve is the path of the point at the center of the flat part of the truncated ball, and the black curve corresponds to the path of the tip of the probe. Figure 4(b) shows the components of the net force on the ball (upper) and the components of the torque (lower). The static friction force and the torque are both constant, horizontal vectors which rotate with the ball, so their components show sine-cosine variation. The friction force provides the centripetal force for the circular motion of the center of mass, so it is always radially inwards. The torque is in the direction of the instantaneous velocity, as expected from Eqs. (39)–(40), and causes the continuous change in the angular momentum vector—which is directed radially outwards, for clockwise rolling—needed for the ball to roll in a circle.

B. Approximately straight trajectories

If the ball in Fig. 3 is spun about a vertical axis when it is launched in a horizontal direction, then one might expect

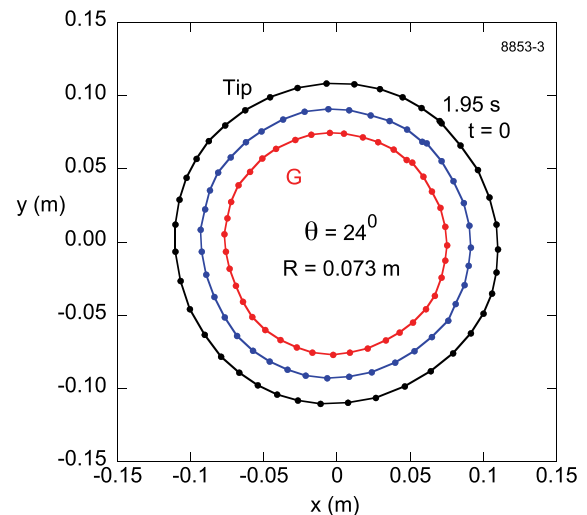Fig. 2. Truncated billiard ball with probe.

Fig. 3. Lawn bowl mode result for the truncated billiard ball showing the trajectories of the tip and base of the probe and the extrapolated coordinates of the center of mass, G, in the horizontal plane. See Supplementary video 8853-3.
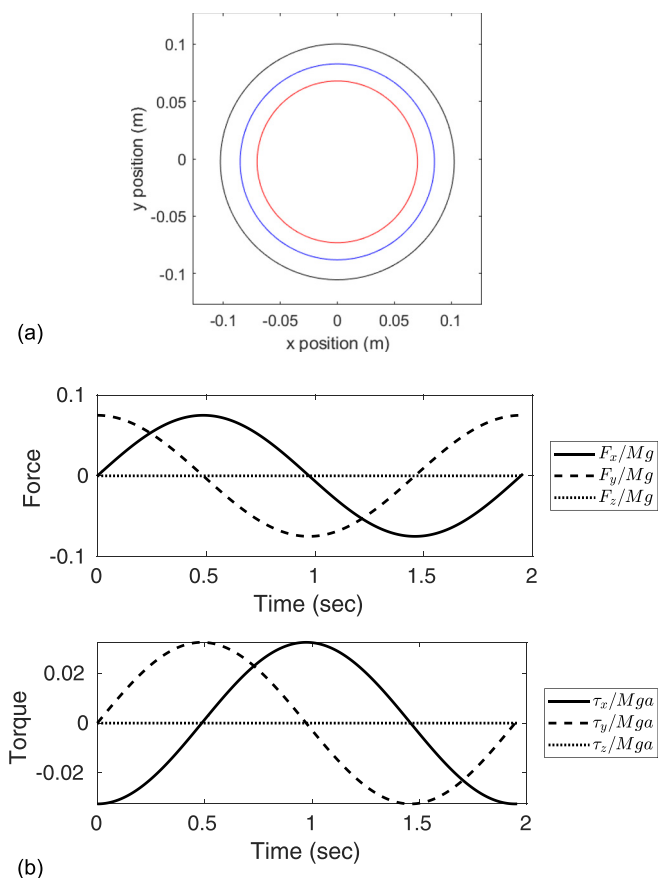
(a)

(b)

Fig. 4. Numerical solution for the lawn bowl mode. Panel (a) shows the trajectory (inner circle: center of mass; middle circle: center of flat section of ball; outer circle: tip of probe), and panel (b) shows the time variation of the net force and torque on the ball.

that it will follow a relatively straight line path on average. If the ball curves initially to the right then it will subsequently curve to the left when the ball rotates to face the opposite direction, as indicated in Fig. 5. That type of behaviour was observed experimentally when the axis of symmetry was horizontal, although the axis did not remain perfectly horizontal throughout the motion. Instead, θ increased and decreased periodically, by about $10°$, with the result that the ball followed a curved path with a large radius of curvature. A typical experimental result is shown in Fig. 6. In this case, there are five precession cycles in 1.35 s, so the average period is 0.27 s and the average precession frequency is $\Omega = 2\pi/0.27 = 23$ rad/s. The angle of the spin axis was observed to vary between about $5°$ below the horizontal, and $20°$ above. If the spin direction was reversed, the ball curved in the opposite direction. In both cases, the ball curved in a retrograde sense.

To reproduce the approximately straight-line motion shown in Fig. 6 with the code, we chose the initial conditions $\dot{\chi}_0 = 23$ rad/s, $\theta_0 = -5°$, and $\dot{\theta}_0 = 0$. The initial spin frequency $\dot{\phi}_0$ needs to be guessed. With the choice $\dot{\phi}_0 = -3$
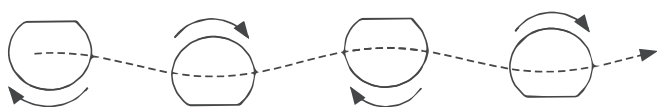

Fig. 5. Assumed path of the truncated ball when it is rotating about a vertical axis, viewed from above.
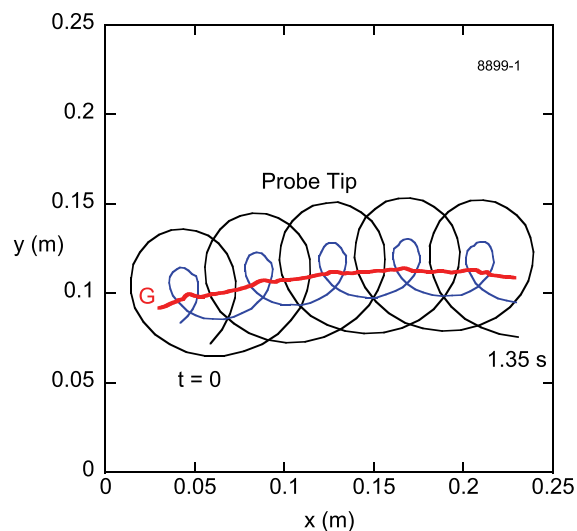

Fig. 6. Approximately straight trajectory showing the paths of the tip and base of the probe and the extrapolated coordinates of the center of mass, G, in the horizontal plane. See Supplementary video 8899-1.

rad/s we obtain the result shown as panel (a) in Fig. 7. We have chosen $\chi_0 = 190°$ to make the overall orientation approximately match Fig. 6. The numerical solution has θ varying between $-5°$ and about $25°$. Panel (b) of Fig. 7 shows the components of the net force on the center of mass of the ball, and the components of the torque about the center
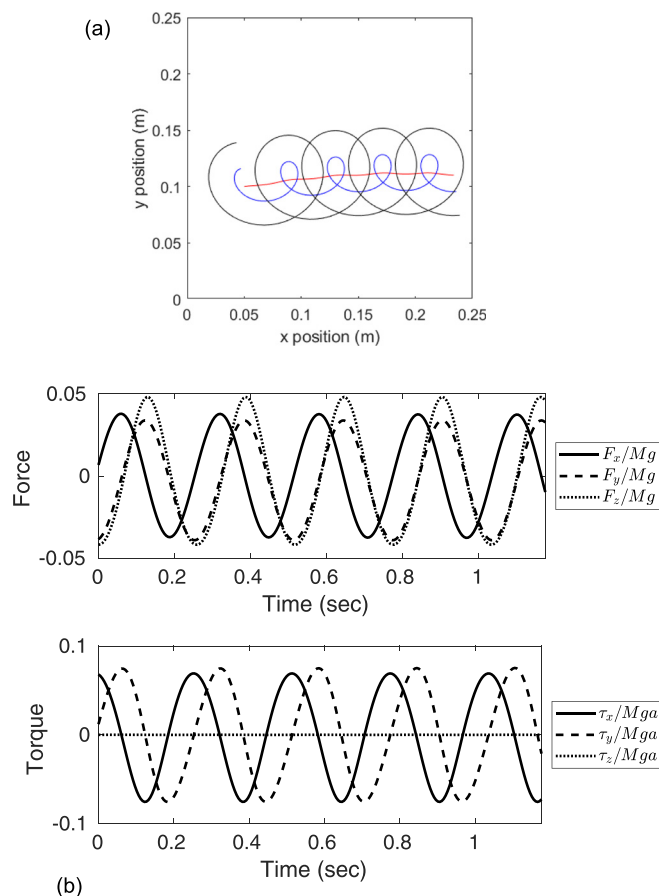
(a)

(b)

Fig. 7. Numerical solution for nearly straight-line motion. Panel (a) shows the trajectory, and panel (b) shows the time variations of the net force and torque on the ball.

of mass. A basic question concerning the motion shown in Fig. 6 is whether the ball is rolling without slipping.

The numerical solution can provide insight. Panel (b) of Fig. 7 indicates that the frictional forces in the numerical solution are less than about $0.05Mg$ in magnitude. This is much smaller than the expected maximum static friction force for the billiard ball on the granite surface, which suggests that the ball is always rolling. Also, panel (b) of Fig. 7 shows that the torque vector is rotating in the x-y plane as the ball precesses. The symmetry of the variation of the horizontal torque accounts for the nearly linear motion of the ball.

C. Approximately circular trajectories

If the initial value of θ is significantly less than 90°, say about 40°, then the large radius of curvature trajectory in Fig. 6 changes to a small radius of curvature trajectory, as shown in Fig. 8 and in supplementary video 8855-1. Large
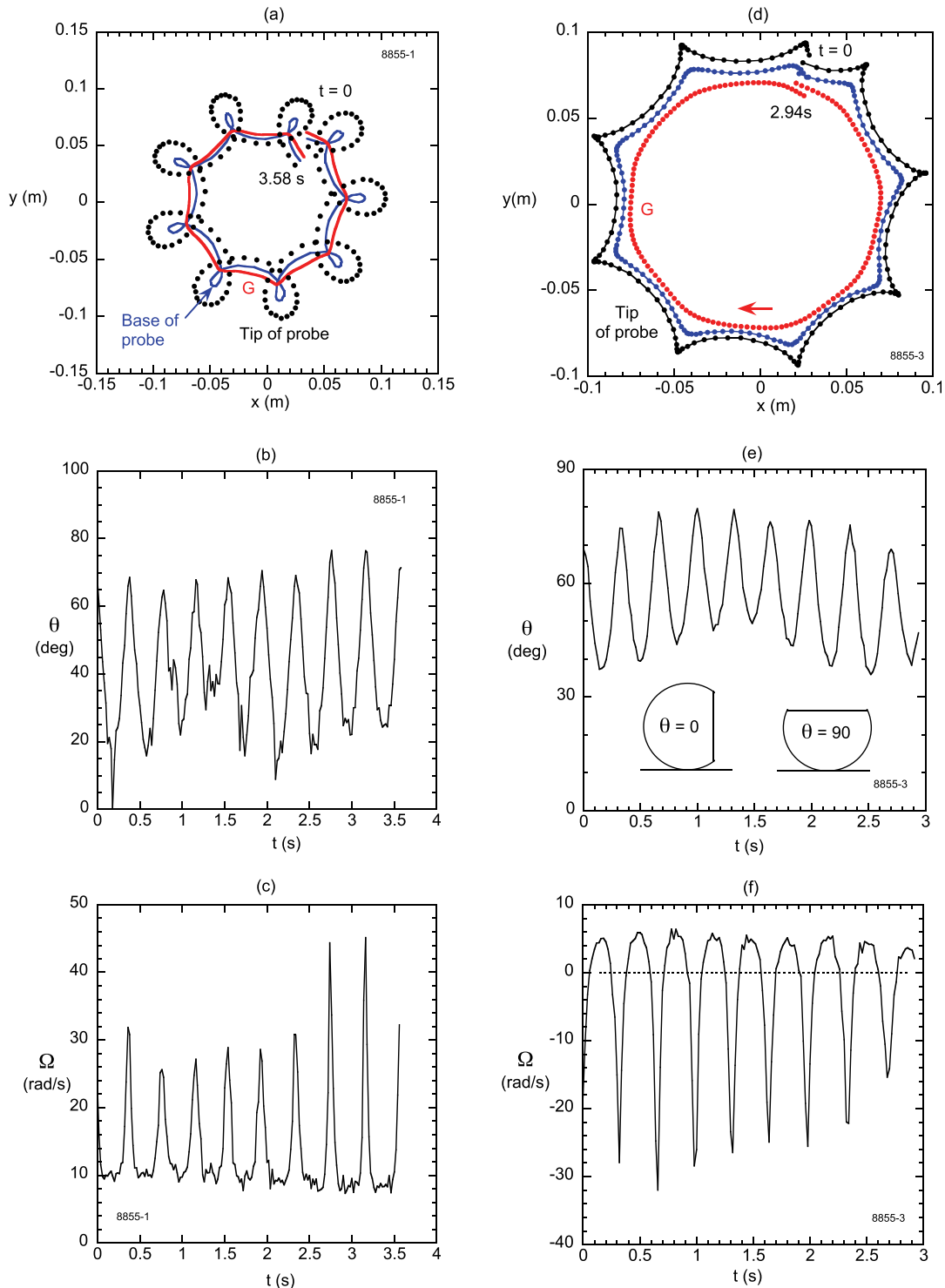

Fig. 8. Two different trajectories (a) and (d) showing the paths of the tip and base of the probe and the extrapolated coordinates of the center of mass, G, in the horizontal plane. The measured variations of θ and Ω for trajectory (a) are shown in (b) and (c). The corresponding graphs of θ and Ω for trajectory (d) are shown in (e) and (f).
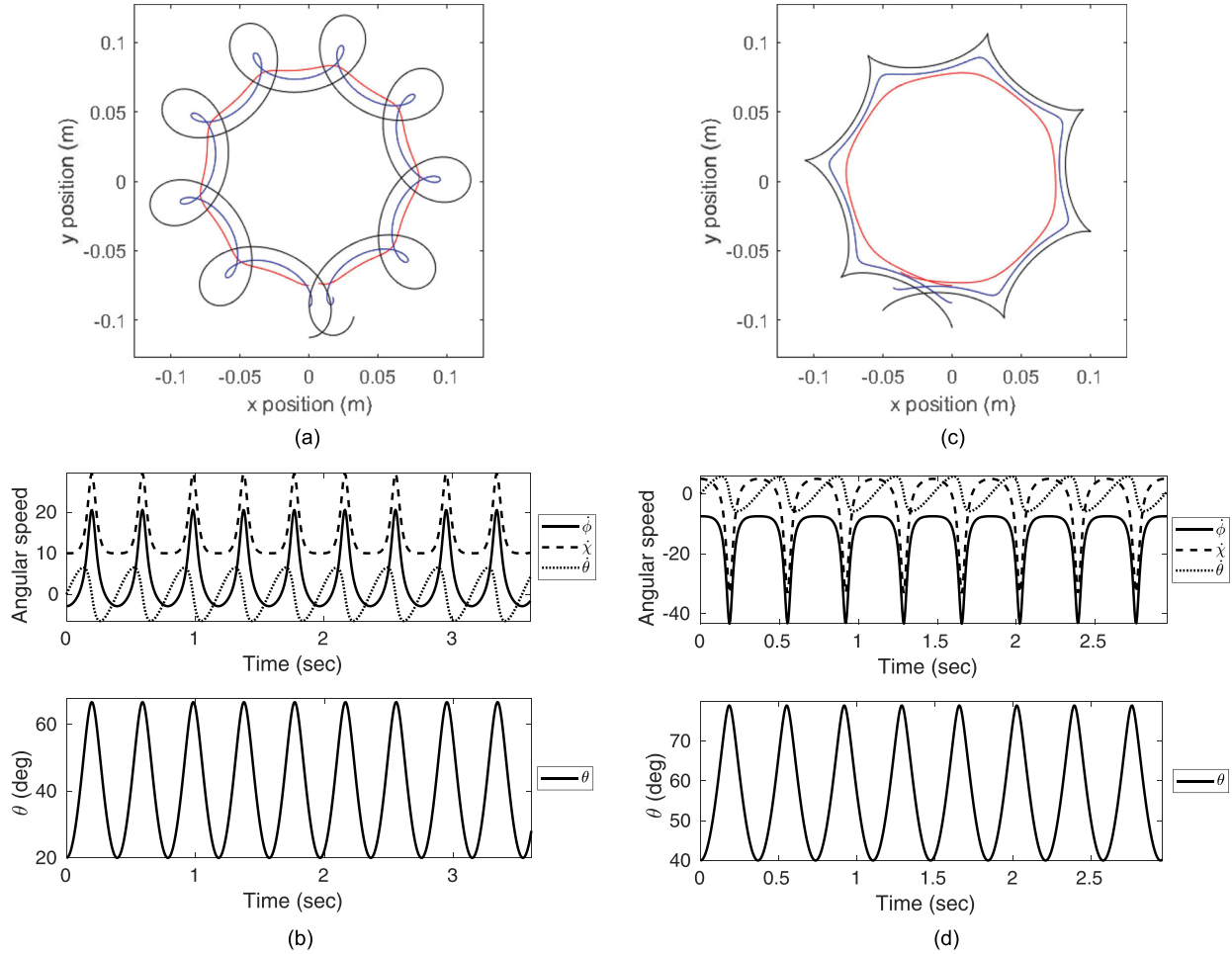
Fig. 9. Numerical solutions with approximately circular trajectories. Panels (a) and (c) show the two trajectories, and panels (b) and (d) show the corresponding time variations of the angular speeds and of θ.

variations in θ are observed during each precession cycle, as well as large variations in Ω. The center of mass rotates in an approximately circular path, in a retrograde sense. However, the local radius of curvature of the path followed by G changes during each precession cycle, in a manner similar to that shown in Fig. 5, depending on whether the flat face of the ball is facing away from or towards the center of the circular path.

To reproduce this motion with the code, we can choose initial conditions based on the plots of θ and Ω versus time in Fig. 8. For example, to attempt to reproduce the case shown in Figs. 8(a)–8(c), we choose $\theta_0 = 20°$, and $\dot{\chi}_0 = 10$ rad/s. After some numerical experimentation, we find that $\dot{\phi}_0 = -2.9$ rad/s gives the motion shown in panel (a) of Fig. 9, for an integration time of 3.6 s. The time variation of $\dot{\chi}$ and θ (as well as $\dot{\theta}$ and $\dot{\phi}$) is shown in panel (b). There is a reasonable match to the data shown in Fig. 8. For the case shown in Figs. 8(d)–8(f), we choose $\theta_0 = 40°$, $\dot{\theta}_0 = 0$, and $\dot{\chi}_0 = 5$ rad/s. Again, we need to guess the spin frequency, and we find that $\dot{\phi}_0 = -7.5$ rad/s gives the motion shown in panel (c) of Fig. 9, for an integration time of 2.95 s. The variation of the angular speeds $\dot{\chi}$, $\dot{\theta}$, and $\dot{\phi}$, as well as of the angle θ is shown in panel (d) of Fig. 9. Once again there is good correspondence with the data in Fig. 8.

Some insight into the approximately circular center-of-mass motion shown in Fig. 9 follows from an inspection of the torque. Figure 10 compares the variation of the torque in

the lawn bowl mode shown in Fig. 4(a) (top panel) with the variation of the torque in the nearly circular case shown in Fig. 9(c) (lower panel). The total time for each plot corresponds to one period of the circular/approximately circular motion. In the lawn bowls case, the torque is horizontal, in the direction of motion, and constant in magnitude [Eqs. (39) and (40)]. The torque causes the change in angular
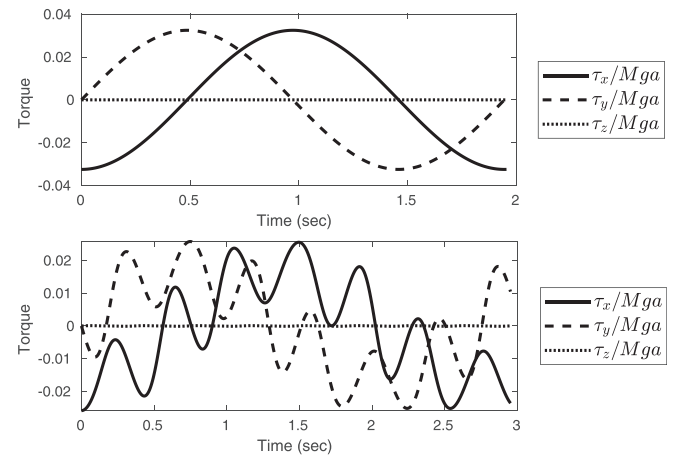

Fig. 10. Variation of torque with time in the lawn bowl mode shown in Fig. 4(a) (top panel) and in the nearly circular trajectory shown in Fig. 9(c) (lower panel).
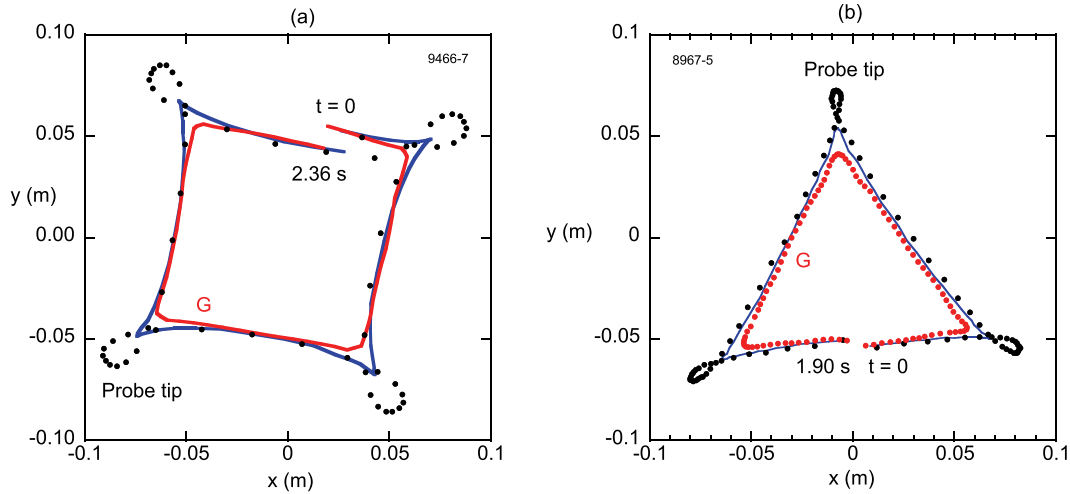
Fig. 11. Trajectories in the horizontal plane, observed at relatively low values of Ω, which demonstrate rolling around a square, and rolling around a triangle. Data points for the probe tip are shown at intervals of 0.04 s. See Supplementary video 9466-7.

momentum needed for the ball to roll in a circle. In the nearly circular motion case, the average variation in the torque has the same pattern, but superimposed on this average variation are oscillations corresponding to the precession of the rolling ball.

D. Low Ω trajectories: Rolling along a square

Even though the paths of the center of mass are approximately circular in Fig. 8, results at low Ω can have distinctly non-circular paths, as demonstrated in Fig. 11. In particular, Fig. 11(a) presents the unexpected result that, for certain initial choices of Ω and θ, it is possible for the biased sphere to roll along a nominally square path! During the motion θ varies from about 0° to about 90° during each precession cycle, with the extreme value achieved at the corners of the square. A supplementary video makes this clear. Figure 11(b) also shows that, for other initial conditions on the motion, the trajectory of the center of mass can also be approximately triangular. During these motions, the loops

followed by the tip of the probe can be relatively large [as they are in Fig. 8(a)] or simple cusp points [as in Fig. 8(b)].

Numerical solutions which approximately match these results are shown in Fig. 12. Although the precession frequency is low on average over the motion, the spin frequencies $\dot{\chi}$ and $\dot{\phi}$ achieve large values at the corners of the shapes, and the angle θ changes rapidly at these locations. The initial conditions producing these trajectories are given in the caption to the figure.

VII. CONCLUSION

A biased ball that rolls without slipping on a horizontal surface can do so in a wide variety of ways. The simplest involves steady state motion in a circular path, where the axis of symmetry remains approximately horizontal, corresponding to a lawn bowl mode. The motion can be described analytically and can be understood intuitively from the fact that the rate of change of angular momentum is equal to the torque acting about the center of mass.
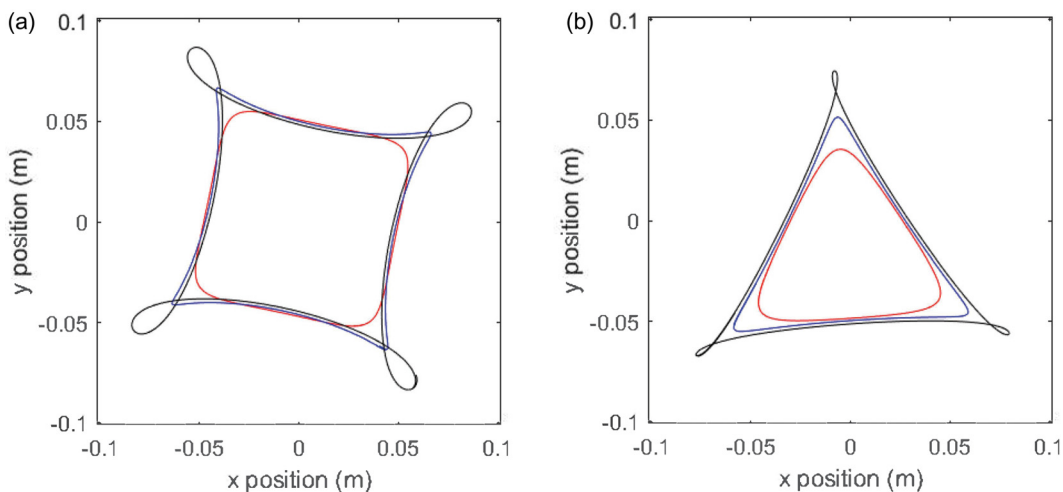

Fig. 12. (a) Rolling around a square, and (b) rolling around a triangle. The initial conditions are: (a) $\theta_0 = -5°$, $\dot{\theta}_0 = 0$, $\dot{\chi}_0 = 4.05$ rad/s, and $\dot{\phi}_0 = -3$ rad/s; (b) $\theta_0 = -10°$, $\dot{\theta}_0 = 0$, $\dot{\chi}_0 = 2.3$ rad/s, and $\dot{\phi}_0 = -2.5$ rad/s.

If the lawn bowl mode is modified by imposing spin about a vertical axis through the center of mass, then the result is also intuitive. That is, the ball curves alternatively to the left and then to the right due to the alternating torque. As a result, the center of mass follows a path that is relatively straight, but it curves slightly in a retrograde sense.

If the axis of symmetry is not horizontal, then motion of the ball is more complex and so are the relevant equations of motion. In general, the axis of symmetry oscillates up and down in a vertical plane while simultaneously precessing about a vertical axis through the center of mass. Furthermore, the center of mass follows a path that is approximately circular if the average precession frequency is large, but which can be approximately triangular or square or many-sided if the average precession frequency is relatively low. The center of mass rotates in a retrograde sense, opposite to the direction of rotation of the precessing ball. The average precession frequency is easily controlled experimentally, simply by spinning the ball about a vertical axis at any desired speed. Similarly, the initial angle of inclination of the axis of symmetry is easily controlled, but the subsequent angle is determined by the precession frequency and the rolling condition.

The ability of the ball to roll along a square path is a curious result, which should appeal to all students of physics. More generally, the motion of a rolling biased ball presents a wonderful topic for student projects—and in fact, this article originated in a semester-long undergraduate project. On the theory side, the description of the motion introduces students to Euler angles, and the derivation of the equations of motion using the Lagrangian approach (or directly using forces and torques) is a problem that is challenging but accessible to junior undergraduates. The experimental investigation of the motion tests laboratory skills, has scope for creativity, and allows students to directly connect the theory with the unexpected behaviour of the ball.

ACKNOWLEDGMENT

APPENDIX A: DERIVATION OF THE EQUATIONS OF MOTION

We use a Lagrangian approach to derive the equations of motion, following Brearley.[2] However, our derivation is exact, whereas Brearley made approximations relevant for a lawn bowl.

Equations (6)–(8) represent constraint relations for the motion. Variations in the coordinates are related by

$$\delta x - a\cos\theta\cos\chi\,\delta\phi + c\cos\theta\cos\chi\,\delta\chi$$
$$+ (a - c\sin\theta)\sin\chi\,\delta\theta = 0, \tag{A1}$$

$$\delta y - a\cos\theta\sin\chi\delta\phi + c\cos\theta\sin\chi\,\delta\chi$$
$$- (a - c\sin\theta)\cos\chi\,\delta\theta = 0, \tag{A2}$$

$$\delta z + c\cos\theta\,\delta\theta = 0, \tag{A3}$$

which represent a set of constraints

$$\sum_{r=1}^{6} A_{rj}\delta q_r \quad (j = 1, 2, 3), \tag{A4}$$

where the q_r denote the six coordinates x, y, z, θ, χ, and ϕ.

The Lagrange equations may be written[2,15] as

$$\frac{\mathrm{d}}{\mathrm{d}t}\left(\frac{\partial T}{\partial \dot{q}_r}\right) - \frac{\partial T}{\partial q_r} - Q_r + \sum_{j=1}^{3}\lambda_j A_{rj} = 0,$$
$$\text{where} \quad r = x, y, z, \theta, \chi, \phi. \tag{A5}$$

The term Q_r denotes the generalised force corresponding to coordinate r, and $\sum_{j=1}^{3}\lambda_j A_{rj}$ represents the forces associated with the constraints. The λ_j are Lagrange multipliers, and the A_{rj} are defined in Eq. (A4). The constraint forces do no work: The only generalised force (which does work) is

$$Q_\theta = -\frac{\partial V}{\partial \theta} = Mgc\cos\theta. \tag{A6}$$

The six Lagrange equations together with the three constraint equations represent nine equations in the nine unknowns (the generalized coordinates plus the Lagrange multipliers). The Lagrange equations are

$$M\ddot{x} + \lambda_1 = 0, \tag{A7}$$

$$M\ddot{y} + \lambda_2 = 0, \tag{A8}$$

$$M\ddot{z} + \lambda_3 = 0, \tag{A9}$$

$$A\ddot{\theta} + A\sin\theta\cos\theta\,\dot{\chi}^2 + B(\dot{\phi} - \dot{\chi}\sin\theta)\cos\theta\,\dot{\chi} - Mgc\cos\theta$$
$$+ (a - c\sin\theta)(\lambda_1\sin\chi - \lambda_2\cos\chi) + \lambda_3 c\cos\theta = 0, \tag{A10}$$

$$(A\cos^2\theta + B\sin^2\theta)\ddot{\chi} - B\sin\theta\,\ddot{\phi} + 2(B - A)\sin\theta\cos\theta\,\dot{\theta}\,\dot{\chi}$$
$$- B\cos\theta\,\dot{\theta}\,\dot{\phi} + (\lambda_1\cos\chi + \lambda_2\sin\chi)c\cos\theta = 0, \tag{A11}$$

$$-B\sin\,\ddot{\chi} + B\ddot{\phi} - B\cos\theta\,\dot{\theta}\dot{\chi}$$
$$- a\cos\theta(\lambda_1\cos\chi + \lambda_2\sin\chi) = 0. \tag{A12}$$

Eliminating λ_1, λ_2, and λ_3 using Eqs. (A1)–(A3) gives the three equations describing the evolution of the Euler angles, namely, Eqs. (13)–(15).

APPENDIX B: FORM OF THE EQUATIONS OF MOTION FOR NUMERICAL SOLUTION

To solve the equations of motion numerically, we require the angular accelerations $\ddot{\theta}$, $\ddot{\chi}$, and $\ddot{\phi}$. The accelerations are evaluated from the other dependent variables using Eqs. (13)–(15) in the form

$$\ddot{\theta} = \frac{\cos\theta}{A + M(a^2 - 2ac\sin\theta + c^2)}$$
$$\times \left\{ Mac\,\dot{\theta}^2 + [(B - A)\sin\theta + Mca']\,\dot{\chi}^2 \right.$$
$$\left. - (B + Maa')\dot{\phi}\dot{\chi} + Mgc \right\}, \tag{B1}$$

where $a' = a - c\sin\theta$, together with

$$\Gamma\boldsymbol{g} = \boldsymbol{h}, \tag{B2}$$

where

$$\Gamma = \begin{pmatrix} (A+Mc^2)\cos^2\theta + B\sin^2\theta & -B\sin\theta - Mac\cos^2\theta \\ -B\sin\theta - Mac\cos^2\theta & B + Ma^2\cos^2\theta \end{pmatrix},$$

(B3)

$$\mathbf{g} = \begin{pmatrix} \ddot{\chi} \\ \ddot{\phi}, \end{pmatrix},$$

(B4)

and

$$\mathbf{h} = \cos\theta \begin{pmatrix} -[2(B-A-Mc^2)\sin\theta + Mac]\dot{\theta}\dot{\chi} \\ + (B - Mac\sin\theta)\dot{\theta}\dot{\phi} \\ (B - 2Mac\sin\theta + Ma^2)\dot{\theta}\dot{\chi} \\ + Ma^2\sin\theta\,\dot{\theta}\dot{\phi} \end{pmatrix}.$$

(B5)

The linear system of Eqs. (B2)–(B5) is solved at each time step. As mentioned in Sec. IV, all equations are implemented in code in a non-dimensional form, with lengths divided by a, times divided by $\sqrt{a/g}$, and moments of inertia divided by Ma^2.

When $\theta = 90°$, the matrix system Eqs. (B2)–(B5) is singular. In this configuration, the axes η and z used to describe $\dot{\phi}$ and $\dot{\chi}$ are parallel, so the chosen axes and angles cannot instantaneously describe three-dimensional rotation. In practice, this is not a significant problem: All of the solutions depicted in this article avoid $\theta = 90°$.

a)Electronic mail: michael.wheatland@sydney.edu.au
b)Electronic mail: rodney.cross@sydney.edu.au

[1]M. N. Brearley and B. A. Bolt, "The dynamics of a bowl," Q. J. Mech. Appl. Math. **11**, 351–363 (1958).

[2]M. N. Brearley, "The motion of a biased bowl with perturbing projection conditions," Math. Proc. Cambridge Philos. Soc. **57**, 131–151 (1961).

[3]Rod Cross, "The trajectory of a ball in lawn bowls," Am. J. Phys. **66**, 735–738 (1998).

[4]David P. Jackson, David Mertens, and Brett J. Pearson, "Hurricane balls: A rigid-body-motion project for undergraduates," Am. J. Phys. **83**, 959–968 (2015).

[5]H. K. Moffatt, Y. Shimomura, and M. Branicki, "Dynamics of an axisymmetric body spinning on a horizontal surface. I. Stability and the gyroscopic approximation," Proc. R. Soc. London A **460**, 3643–3672 (2004).

[6]Rod Cross, "Spin experiments with a biased ball," Eur. J. Phys. **40**, 055003 (2019).

[7]A. Kilin and E. Pivovarova, "The rolling motion of a truncated ball without slipping and spinning on a plane," Regul. Chaotic Dyn. **22**, 298–317 (2017).

[8]M. A. Jalali, M. S. Sarebangholi, and M.-R. Alam, "Terminal retrograde turn of rolling rings," Phys. Rev. E **92**, 032913 (2015).

[9]A. V. Borisov, A. A. Kilin, and Y. L. Karavaev, "Retrograde motion of a rolling disk," Phys. Usp. **60**, 931–934 (2017).

[10]Cliff Frohlich, "What makes bowling balls hook?," Am. J. Phys. **72**, 1170–1177 (2004).

[11]Kevin King, N. C. Perkins, Hugh Churchill, Ryan McGinnis, Ryan Doss, and Ron Hickland, "Bowling ball dynamics revealed by miniature wireless MEMS inertial measurement unit," Sports Eng. **13**, 95–104 (2011).

[12]Rod Cross, "A hemispherical tippe top," Eur. J. Phys. **41**, 025001 (2020).

[13]W. H. Press, B. P. Flannery, S. A. Teukolsky, and W. T. Vetterling, *Numerical Recipes in C*, 2nd ed. (Cambridge U. P., New York, 1992).

[14]See supplementary material at http://dx.doi.org/10.1119/10.0000905 for movies of the motion of the truncated billiard ball filmed at 300 fps. The visualisations produced by the code, as well as the supplementary videos, are at <http://www.physics.usyd.edu.au/~wheat/biased-ball/>.

[15]E. T. Whittaker, *A Treatise on the Analytical Dynamics of Particles and Rigid Bodies*, 2nd ed. (Cambridge U. P., Cambridge, UK, 1917).

Lissajous Figure Demonstration

A circle can be regarded as a Lissajous figure formed when two simple harmonic oscillations of the same frequency and amplitude are added perpendicularly to each other – with a phase difference of 90°. This device is designed to fit into the gate of a standard North American lantern slide projector with a 3.25 in. by 4 in. viewing area. It can also be used on an overhead projector. This beautiful little piece of demonstration apparatus is at Ohio Wesleyan University in Delaware, Ohio. (Picture and text by Thomas B. Greenslade, Jr., Kenyon College)